



Cite this: *RSC Adv.*, 2025, 15, 48498

High-efficiency and environmentally friendly copper recovery from waste copper clad laminate and its pyrolysis behavior through a novel low-temperature rotary furnace process

Meng Tian  and Xianglan Zhang*

Recycling metal materials from waste copper clad laminate (WCCL) in a pollution-free and efficient way holds significance for the comprehensive utilization of resources. This study used waste paper-laminated copper clad laminate (PL-WCCL) as a raw material and conducted pyrolysis in a rotary furnace. The variations of the functional groups in PL-WCCL and the non-metallic part of PL-WCCL under different conditions were analyzed by thermogravimetric coupled Fourier transform infrared spectroscopy (TG-FTIR). The liquid-phase products were analyzed using gas chromatography-mass spectroscopy (GC-MS), and the morphology of the solid-phase products and the contact surfaces of the metal and non-metal parts of PL-WCCL were determined by photography and scanning electron microscopy-energy dispersive X-ray spectroscopy (SEM-EDS). The results indicate that the maximum weight loss rate of PL-WCCL is 62.48%, and the activation energy (E) is 29.84 kJ mol⁻¹. During the pyrolysis, copper can lower the beginning reaction temperature, facilitate the release of bromine and chlorine, accelerate the synthesis of lighter hydrocarbons, and increase the release of CO₂. The optimal conditions are as follows: a retention time of 60 min at 150 °C and a filling capacity of 51.95 g L⁻¹, resulting in a 100% separation rate of metal, without requiring crushing. The liquid organic products obtained were merely phenol and o-cresol. This research introduced a comprehensive green processing method utilizing a rotary furnace as the reactor to effectively extract metallic copper from PL-WCCL.

Received 11th September 2025
Accepted 24th November 2025

DOI: 10.1039/d5ra06865g

rsc.li/rsc-advances

1 Introduction

Copper clad laminate (CCL) is manufactured by saturating reinforcing materials, such as wood pulp paper or glass fiber, with epoxy resin and halogen flame retardant, followed by applying copper foil to one or both sides and subjecting the assembly to heat and pressure treatments. It serves as a fundamental component in the production of printed circuit boards (PCBs).¹ Based on the choice of reinforcing materials, CCL can mainly be categorized into glass fiber-reinforced copper clad laminate (FR-CCL) and paper-laminated copper clad laminate (PL-CCL).² As the world's largest producer of CCL, China is expected to increase its production volume to 1.17 billion m² by 2025,³ and waste copper clad laminate (WCCL), namely, the offcut generated during the manufacturing, would account for over 10% of the total yield.⁴ WCCL without electronic components has a copper content of approximately 10% to 20%,⁵ which is much higher than the grade of the original copper ore. It is thus called an "urban mine".⁶

Various technologies, including physical method,⁷ organic solvent swelling method,⁸ hybrid processes⁹ and pyrolysis

method,¹⁰ have been employed to recycle copper from waste copper clad laminate (WCCL). Both the organic solvent swelling method and the hybrid process method are confined to laboratory studies and have not been utilized for large-scale recycling activities. It is the physical method that is widely adopted in industries for the recovery of copper. However, the recovery of the metal *via* the physical method typically involves shattering the sheet material into smaller pieces or even powder,^{11,12} and the metal is separated from non-metals under shear forces during this process, achieving a metal-recovery efficiency ranging from merely 65% to 90%.¹³ However, the recovery of the metal *via* the physical method involves a relatively large number of subsequent steps. Besides, if the reinforcing materials of the WCCL are wood pulp papers, it tends to adhere to the crushing machinery, which complicates the separation process of metals from non-metals and hinders the efficient recycling of metals from waste paper-laminated copper clad laminate (PL-WCCL).¹⁴

Pyrolysis, which is a potential technology and commonly used in recovering metals from WCCL, breaks down high-molecular polymers and destroys the bonding force between metals and non-metals of WCCL through heating, facilitating the separation of the metal and improving the metal recovery rate.¹⁵ Further, while generating high-value hydrocarbons, this technology significantly reduces the volume and recovers more

School of Chemical and Environmental Engineering, China University of Mining and Technology (Beijing), No. Ding 11, Xueyuan Road, Haidian District, Beijing 100083, PR China. E-mail: zhxl@cumt.edu.cn; Tel: +86-135-2170-3609



energy.¹⁶ However, the halogen flame retardants contained in non-metal materials in WCCL commence decomposition at 280 °C,¹⁷ potentially generating persistent organic pollutants (POPs), such as poly-brominated diphenyl ethers (PBDEs), presenting health and safety hazards to humans and the environment.¹⁸ The inadequate handling of POPs may severely contaminate the ecological environment.^{19,20} Therefore, investigating effective approaches to separate and recover metals from PL-WCCL, as well as mitigating the environmental impact associated with non-metal parts, holds considerable practical value for the resourceful utilization of PL-WCCL.

The design and selection of the reactor, along with the control and modulation of experiment conditions, exert a significant influence on the separation efficiency of metals and non-metals in PL-WCCL *via* pyrolysis. There are relatively few studies that explicitly use large-sized PL-WCCL as the experimental material and conduct research on metal separation *via* pyrolysis. For example, Liu *et al.* conducted pyrolysis of PL-WCCL at 300 °C in a fixed-bed reactor. After that, the metal separation rate reached 100%, indicating that intact copper foil sheets could be manually stripped.²¹ CCL is the fundamental component in the production of PCBs. From the perspective of composition, WCCL can almost be regarded as the same material as WPCBs without electronic components. Thus, the research regarding the separation of metals and non-metals of WPCBs through pyrolysis can be referenced.

Researchers have employed the fixed-bed reactor to conduct the pyrolysis of large-sized WPCB without electronic components and investigated the variation of the metal separation rate by controlling the temperature, reacting atmosphere and retention time.

Yan G. *et al.*²² conducted pyrolysis treatment on waste printed circuit boards (WPCBs). At 200 °C, the copper separation rate reached 85.66%. Kim B. *et al.*²³ performed pyrolysis treatment on WPCBs and found that copper was enriched in the raw materials, with large particle sizes obtained at 300 °C. Chen Y. *et al.*¹³ carried out pyrolysis treatment on WPCBs and obtained a copper recovery rate of 92.38% at 330 °C. Guo X. *et al.*²⁴ conducted pyrolysis treatment on WPCBs and found that at 500 °C, the metal and non-metal parts could be manually peeled apart. Long L. *et al.*²⁵ performed pyrolysis treatment on WPCBs and found that at 550 °C, copper was enriched in the raw material particles with particle sizes larger than 0.45 mm, and the separation rate was approximately 99%. However, Ma H. *et al.*²⁶ found that when performing pyrolysis treatment on WPCBs at 800 °C in a fixed-bed reactor equipped with a stirring function, the copper foil and non-metal parts could be automatically separated after the pyrolysis process was completed.

Current studies on the separation the metals and non-metals of WPCBs reveal that conducting the pyrolysis process under a fixed temperature range of 200 to 550 °C for 30 to 120 min in a fixed-bed reactor, whether in an air atmosphere, nitrogen atmosphere, or vacuum, enables easier separation of metals and non-metals and increases the metal recovery rate. However, after the pyrolysis process, further crushing, screening, sorting, or manual peeling is necessary. The addition of the stirring function to the fixed-bed reactor is conducive to the separation of the copper foil and non-

metals, eliminating the need for further crushing and manual peeling. However, the above-mentioned literature studies did not address the release of non-metallic pollutants during the pyrolysis process. Currently, studies on the separation of metals and non-metals from WPCB or WCCL are mainly carried out in fixed-bed reactors, and there are no public reports on rotary furnaces.

The rotary furnace is a common type of industrial furnace. The materials within it rotate along with the furnace body under the drive of the blades. After rising to the highest point, the materials return to the bottom of the rotary furnace along the furnace bed.²⁷ In a rotary furnace, the materials not only rotate but also undergo translation and collision,²⁸ and these vigorous movement enhances the flow and heat transfer of the materials, ensuring thorough mixing.²⁹ Moreover, rotary furnaces have a simple structure and wide adaptability to different types and sizes of raw materials while being convenient to operate. In pyrolysis experiments using the rotary furnace, most researchers adjust the parameters, such as the temperature, rotation speed, inclination angle of the reactor, particle size of the raw materials, and gas flow rate. The aim is to make the yield and composition of the final pyrolysis products comparable to those obtained when using a fluidized-bed reactor.²⁸ Zhu Y. *et al.*³⁰ designed a pilot-scale rotary kiln pyrolysis furnace featuring a hierarchical condensation function. By applying the method of controlling variables, they analyzed the impacts of temperature, moisture content of materials, and condensate water flow rate on the distribution of three-phase pyrolysis products of waste printed circuit boards (WPCBs).

Therefore, this study aims to capitalize on the prominent advantages of the rotary furnace to explore the optimal conditions for the automatic separation of metals and non-metal parts of PL-WCCL during the pyrolysis. Additionally, it endeavors to recycle metals with lower energy consumption by streamlining the technological process. Meanwhile, through the analysis of the distributions of gas, liquid, and solid-phase products at different pyrolysis temperatures and the composition of the liquid-phase products, secondary pollution resulting from the decomposition of halogen-containing flame retardants can be circumvented. In comparison with conventional physical methods for metal separation and recovery, the proposed method can ensure a relatively high separation efficiency while significantly reducing the number of subsequent separation process steps. It thus lays the foundation for the “green recycling”³¹ industry of metals and non-metals in PL-WCCL.

2 Materials and methods

2.1 Raw materials

The PL-WCCL used as raw material in our study was collected from Guangzhou Jiantao Chemical Trade Company. This PL-WCCL is a substrate of a waste print circuit board with uniform thickness, made by laminating insulating paper as the reinforcing material, epoxy resin, and copper foil. The compositions of PL-WCCL are shown in Fig. 1. The PL-WCCL was cut into 4 cm × 2 cm pieces for standby.

30.000 g of PL-WCCL was taken, and the copper foil and non-metal parts were separated manually and weighed separately.



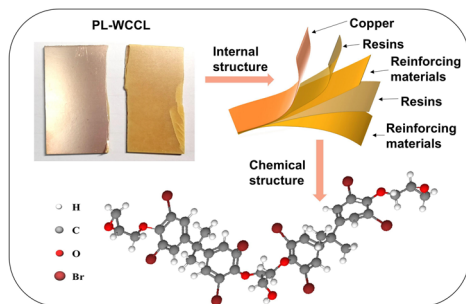


Fig. 1 Schematic of the compositions of the PL-WCCL.

The contents of metals and non-metals contained in the PL-WCCL are 3.2056 g and 26.7964 g. The content of Cu in PL-WCCL was calculated to be 11%.

Elemental analysis and X-ray fluorescence (XRF) analysis were conducted on the non-metallic part of waste paper laminated-copper clad laminate (PL-NMWCCCL), and the experimental results are listed in Tables 1 and 2, respectively. Table 1 shows that the content of carbon in PL-NMWCCCL is 46.22%, indicating a high content of organic matter. In Table 2, the contents of chlorine and bromine in PL-NMWCCCL account for 80% of all the elements measured, and the content of chlorine is about twice that of bromine.

2.2 Experimental devices and steps in the pyrolysis

The schematic illustration of the rotary furnace pyrolysis device is shown in Fig. 2. The furnace consists of a nitrogen (N_2) cylinder, rotary furnace, liquid condensation collector, and gas bag. The gas produced during the pyrolysis process is collected by the gas bag, the liquid is collected after condensation through the condenser, and the solid is discharged from the furnace tube after the experiment.

(1) The influence of the pyrolysis temperature and time: about 30 g of PL-WCCL with a particle size of 4 cm \times 2 cm (the corresponding number of filling blocks is denoted as Q_0) was placed in the rotary furnace. N_2 gas (99.9%) was injected into the rotary furnace at a flow rate of 100 mL min^{-1} , and the rotation speed was 2.44 rpm. The pyrolysis temperature was raised at a rate of 5 $^\circ\text{C min}^{-1}$ to varying final temperatures (150, 200, 250, 300, and 350 $^\circ\text{C}$), and the retention time was set to 30 min or 60 min.

(2) The influence of the varying amounts of PL-WCCL added: with the pyrolysis temperature fixed at the temperature required to achieve the above-mentioned optimal metal separation rate and a retention time of 60 min, the separation status of metal and non-metal under the conditions of varying raw material amounts of 50 g, 100 g, and 150 g was investigated.

(3) Comparison between rotary furnaces and fixed furnaces: at the temperature corresponding to the aforementioned

Table 2 XRF analysis of the PL-NMWCCCL

Element	Relative content %	Element	Relative content %
Br	29.837	Fe	1.222
P	2.815	Ca	0.552
Cr	2.241	S	0.249
Al	1.971	Na	0.225
Si	1.715	Zn	0.025
Cl	49.497		

optimal metal separation rate, 50 g of PL-WCCL was put into a rotary furnace and a fixed furnace, separately, and the retention time was 60 min.

Through statistically counting the quantity Q_1 of metals after complete separation, the metal separation rate was obtained using eqn (1). The yields of the solid and liquid products are calculated by eqn (2) and (3), respectively, and the yield of gas products was obtained using the mass balance eqn (4).

$$S_m = \frac{Q_1}{Q_0} \times 100\% \quad (1)$$

$$Y_s = \frac{M_a}{M_0} \times 100\% \quad (2)$$

$$Y_l = \frac{M_b}{M_0} \times 100\% \quad (3)$$

$$Y_g = 100\% - Y_s - Y_l \quad (4)$$

Among them, S_m represents the metal separation rate; M_0 is the mass of the raw materials added, M_a is the mass of the non-metallic product from pyrolysis, and M_b is the mass of the liquid-phase product from pyrolysis.

The name of the pyrolysis products was designated as “raw material + furnace type + temperature + product form” (The first letter of the word represents itself, like G for gas, S for solid, L for liquid, SI for solid interface between metal part and non-metal part). Regarding the short expression of the raw material, PW is waste paper laminated copper clad laminate (PL-WCCL), MPW represents the metal part of PL-WCCL and NPW is the non-metallic part of waste paper laminated copper clad laminate (PL-NMWCCCL). For instance, $PW-F-150-L$ indicates the liquid product of PL-WCCL after pyrolysis at 150 $^\circ\text{C}$ in a fixed furnace; $NPW-R-300-S$ represents the solid product of PL-NMWCCCL after pyrolysis at 300 $^\circ\text{C}$ in a rotary furnace. When cross-sectional characterization of the solid product is necessary, “CS” is added to the end, like $NPW-R-300-S-CS$.

2.3 Analysis method

Elemental analysis of PL-NMWCCCL was performed using an elemental analyzer (Vario MACRO cube, Germany) and X-ray fluorescence spectrometer (XRF, Axios, PANalytical company, Netherlands). The pyrolysis characteristics and functional groups of PL-WCCL and PL-NMWCCCL were analyzed using thermogravimetry-Fourier transform infrared spectroscopy (TG-FTIR, Bruker ALPHA TENSOR 27, Bruker Company, Germany).

Table 1 Contents of elements in PL-NMWCCCL

C/wt%	H/wt%	O/wt%	N/wt%	S/wt%
46.22	4.02	22.48	4.95	0.13



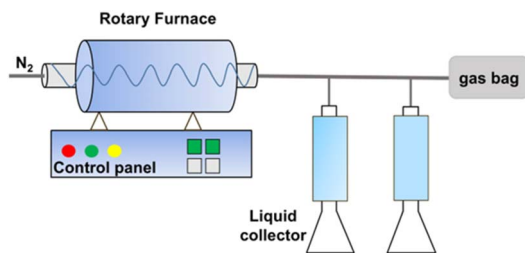


Fig. 2 Schematic of the rotary furnace pyrolysis devices.

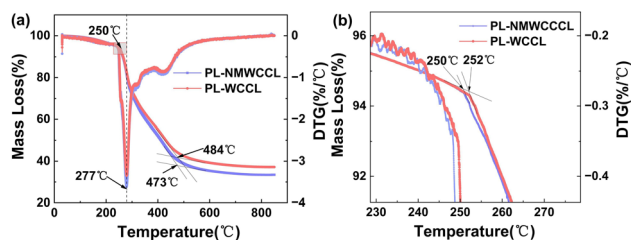


Fig. 3 (a) The TG curve of PL-WCCl and PL-NMWCCl; (b) DTG curve of PL-WCCl and PL-NMWCCl.

The test conditions were as follows: N_2 atmosphere, heating rate of $5\text{ }^\circ\text{C min}^{-1}$, temperature range of $30\text{--}850\text{ }^\circ\text{C}$, and spectral range of $470\text{--}4000\text{ cm}^{-1}$. This experiment used gas chromatography-mass spectroscopy (GC-MS, QP2010, SHIMADZU, Japan) to perform qualitative analysis of the composition in the pyrolysis oil

$$\alpha = \frac{\text{Initial mass of the sample } w_0 - \text{Mass of the sample at time } tw_i}{\text{Initial mass of the sample } w_0 - \text{Mass of the sample at the end of pyrolysis } w_e};$$

and also observed the presence of halogenated organic compounds in the pyrolysis oil. The test conditions were as follows: sample volume of $0.5\text{ }\mu\text{L}$, initial temperature of chromatography column/retention time: $40\text{ }^\circ\text{C}/5\text{ min}$; heating rate of $10\text{ }^\circ\text{C min}^{-1}$, final temperature of $300\text{ }^\circ\text{C}$, retention time of 10 min , carrier gas helium (He) flow rate of 1.0 mL min^{-1} , mass scanning range m/z of $30\text{--}500$, scanning rate of $1\text{ time}/2.6\text{ s}$, vaporization chamber temperature of $280\text{ }^\circ\text{C}$, transmission temperature of $280\text{ }^\circ\text{C}$. A scanning electron microscope (SEM, TESCAN MIRA LMS, TESCAN Company, Czech) was used to test the surface morphology features of the raw materials and the solid phase products after pyrolysis under the following test conditions: accelerating voltage = 15 kV , beam intensity = low beam and spectral line surface scanning, probe mode = backscattering.

3 Results and discussion

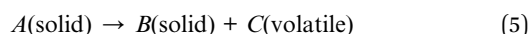
3.1 TG-FTIR analysis of PL-WCCl

3.1.1 Pyrolysis characteristics of PL-WCCl. The pyrolysis characteristics of 1 mm^2 PL-WCCl and PL-NMWCCl were analyzed, respectively, by thermogravimetric analysis (TGA).

The results are shown in Fig. 3, and the pyrolysis characteristic parameters are presented in Table 3.

As shown in Fig. 3, there is no significant difference in the TG curves of PL-WCCl and PL-NMWCCl. The initial decomposition temperature of PL-WCCl is $250\text{ }^\circ\text{C}$ and that of PL-NMWCCl is $252\text{ }^\circ\text{C}$ (Fig. 3b). Regarding the termination decomposition temperature, it is $484\text{ }^\circ\text{C}$ for PL-WCCl and $473\text{ }^\circ\text{C}$ for PL-NMWCCl. The maximum weight loss rate of PL-WCCl is 62.48% and that of PL-NMWCCl is 66.51% . During the pyrolysis, the temperature range of the thermal weight loss of PL-WCCl is broader than that of PL-NMWCCl, suggesting that the metal Cu contained in PL-WCCl has a certain influence on the pyrolysis, although the influence is relatively minor.^{20,32–34}

The PL-WCCl pyrolysis is a relatively complex solid-state thermal decomposition process,³⁵ which can be represented by the following reaction function in eqn (5):



Consequently, the reaction rate equation during the pyrolysis process is eqn (6):

$$\frac{d\alpha}{dt} = k(T)f(\alpha) \quad (6)$$

In the above equation, $k(T)$ is the reaction rate constant, which can be represented by the Arrhenius equation, $k(T) = Ae^{-\frac{E}{RT}}$. $f(\alpha)$ is the reaction mechanism function, α is the conversion rate and can be calculated by

If $f(\alpha) = (1 - \alpha)^n$, $dt = dT/\beta$ (β is the heating rate, K s^{-1}), eqn (6) can be converted into eqn (7):

$$\frac{d\alpha}{dt} = k(T)f(\alpha) = Ae^{-\frac{E}{RT}} \times (1 - \alpha)^n \rightarrow \frac{d\alpha}{f(\alpha)} = \frac{A}{\beta} e^{-\frac{E}{RT}} dT \quad (7)$$

Eqn (7) and (8) are integrated to obtain the following:

$$g(\alpha) = \int_0^\alpha \frac{d\alpha}{f(\alpha)} = \int_0^T \frac{A}{\beta} e^{-\frac{E}{RT}} dT = \frac{AE}{\beta R} p(x) \quad (8)$$

where E is the activation energy (J mol^{-1}), A is the pre-exponential factor ($1/\text{s}$), T is the thermodynamic temperature (K), and R is the universal gas constant ($8.314\text{ J mol}^{-1}\text{ K}^{-1}$).

The Coats-Redfern integration model method is employed to fit and solve eqn (8), which can calculate the kinetic parameters for PL-WCCl pyrolysis in different stages of pyrolysis using a TG curve. The Coats-Redfern integration model method can be expressed as eqn (9):

$$\ln\left(\frac{g(\alpha)}{T^2}\right) = \ln\left(\frac{AE}{\beta R}\right) - \frac{E}{RT} \quad (9)$$



Table 3 Pyrolysis characteristic parameters of PL-WCCL and PL-NMWCCl with a heating rate of 5 °C min⁻¹

Raw materials	Initial temperature/°C	Peak temperature/°C	Final temperature °C	Weight loss/%
PL-WCCL	250	278	484	62.48%
PL-NMWCCl	252	277	473	66.51%

After performing integration on eqn (8), if $n = 1$, the Coats–Redfern function is converted into eqn (10):

$$\ln \left[\frac{-\ln(1-\alpha)}{T^2} \right] = \ln \left[\frac{AR}{\beta E} \left(1 - \frac{2RT}{E} \right) \right] - \frac{E}{RT} \quad (10)$$

If $n \neq 1$, the Coats–Redfern function is converted into eqn (11):

$$\ln \left[\frac{1 - (1-\alpha)^{1-n}}{T^2(1-n)} \right] = \ln \left[\frac{AR}{\beta E} \left(1 - \frac{2RT}{E} \right) \right] - \frac{E}{RT} \quad (11)$$

For the general reaction section and most values of E , $2RT/E \ll 1$; thus, $1 - \frac{2RT}{E} \approx 1$, and eqn (10) and (11) can be simplified as eqn (12) and (13), respectively:

$$\ln \left[\frac{-\ln(1-\alpha)}{T^2} \right] = \ln \left[\frac{AR}{\beta E} \right] - \frac{E}{RT} \quad (12)$$

$$\ln \left[\frac{1 - (1-\alpha)^{1-n}}{T^2(1-n)} \right] = \ln \left[\frac{AR}{\beta E} \right] - \frac{E}{RT} \quad (13)$$

Consequently, $1/T$ is the abscissa, and $\ln[-\ln(1-\alpha)/T^2]$ or $\ln[1 - (1-\alpha)^{1-n}/T^2(1-n)]$ is the ordinate. Fitting the thermogravimetric data through application origin, if the selected reaction order (n value) is correct, a straight line with a slope of $(-E/R)$ and an intercept of $\ln \frac{AR}{\beta E}$ can then be achieved by solving a univariate quadratic equation ($y = kx + b$). Therefore, the pyrolysis activation energy and pre-exponential factor can be derived. The correlation coefficient r^2 , pyrolysis activation energy, and pre-exponential factor calculated by adopting different n values are listed in Table S1.

By employing the C–R method, it was calculated that when the kinetics n of PL-NMWCCl was 1.5, R^2 was 0.98, the activation energy E was 31.95 kJ mol⁻¹, and the pre-exponential factor A was 1.303×10^3 min⁻¹. When the kinetics n of PL-WCCL was 1.5, R^2 was 0.97, the activation energy E was 29.84 kJ mol⁻¹, and the pre-exponential factor A was 5.035×10^2 min⁻¹. The activation energy required for the pyrolysis of PL-WCCL with insulating paper as the substrate was lower than that of FR4-WCCL, with the glass fibres as the substrate (144.11 kJ mol⁻¹).²⁹

3.1.2 3D-FTIR analysis. The 3D-FTIR spectra of the volatile products obtained from the pyrolysis of PL-NMWCCl and PL-WCCL in a N₂ atmosphere within the temperature range of 30–850 °C are depicted in Fig. 4a and b. It can be observed from Fig. 4a and b that the release patterns of the volatile products from PL-NMWCCl and PL-WCCL during pyrolysis are similar, both attaining the maximum release intensity around 288 °C. In the high-wavenumber segment, the color of PL-WCCL is slightly

purple, indicating a relatively small release amount. In the 500–1000 cm⁻¹ region, more gas is released from the pyrolysis of PL-WCCL if the temperature is above 500 °C. The wave peak at 669 cm⁻¹ represents the C–Cl bond; the wave peak at 522 cm⁻¹ represents the C–Br bond.³⁷ Hence, Fig. 4c and d show comparisons of the FTIR spectra of the C–Cl and C–Br bonds at different temperatures. It can be seen that the release intensity of the C–Cl bond in PL-NMWCCl is 0.0088 a.u. at 288 °C, and the release intensity of the C–Br bond in PL-NMWCCl is 0.0033 a.u. at 284 °C. The release intensity of the C–Cl bond in PL-WCCL is 0.0201 a.u. at 287.4 °C, and the release intensity of the C–Br bond in PL-WCCL is 0.0036 a.u. at 283 °C. This suggests that the presence of Cu facilitates the transformation of bromides and chlorides, enabling more of them to decompose from PL-WCCL during the pyrolysis process.³⁸

Fig. 5 presents the FTIR curves of the volatile products resulting from the pyrolysis at various temperatures. From Fig. 5a and b, the infrared peak intensities of both PL-NMWCCl and PL-WCCL reach the maxima at 300 °C. The peaks at 750 cm⁻¹ and 2933 cm⁻¹ are likely attributed to the presence of $-(CH_2)_n-$, with $n \leq 3$. When combined with the peaks at 1195 cm⁻¹, 1364 cm⁻¹, and 1394 cm⁻¹, it can be deduced that there exists an isopropyl structure, $-\text{CH}(\text{CH}_3)_2$.³⁹ The peaks at 1512 cm⁻¹, 1542 cm⁻¹, and 1554 cm⁻¹ are characteristic of the C=C bond vibration of the benzene ring. The C–H bond vibration wave peaks of the benzene ring, $-\text{C}_6\text{H}_5$, at 1700–1769 cm⁻¹ and 795 cm⁻¹ could highlight that the substitution on the benzene ring is of the 1, 3, 5, 6 type.⁴⁰ The peak at

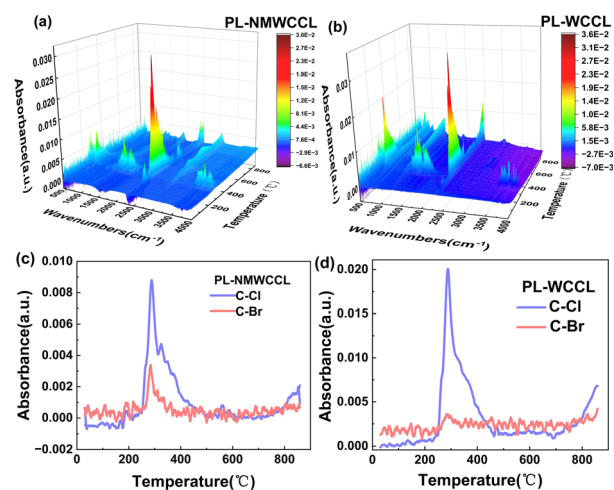


Fig. 4 3D-FTIR spectra of the volatile products at 30–850 °C: (a) PL-NMWCCl and (b) PL-WCCL. FTIR curves of the C–Cl bond and C–Br bond at various temperatures: (c) PL-NMWCCl and (d) PL-WCCL.



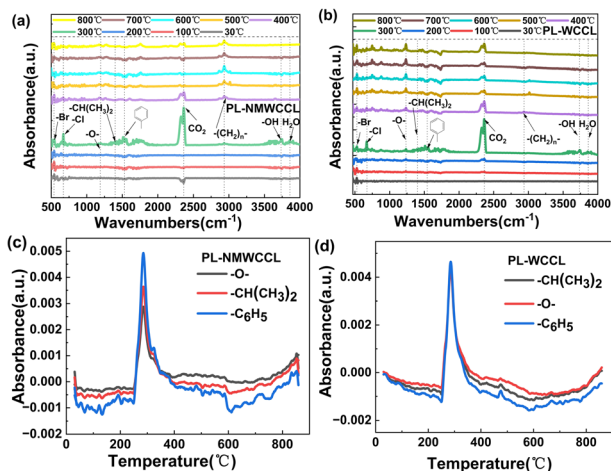


Fig. 5 FTIR of the volatile products at 30–850 °C: (a) PL-NMWCCl and (b) PL-WCCl. Variations of three functional groups at 30–850 °C: (c) PL-NMWCCl and (d) PL-WCCl.

1233 cm⁻¹ corresponds to the C–O bond stretching vibration of the fatty ether, while the peak at 1064 cm⁻¹ is the C–O bond stretching of the benzyl ether molecular skeleton.

The variations of the above-mentioned three functional groups within the temperature range of 30–850 °C are depicted in Fig. 5c and d. It can be observed that for PL-NMWCCl, the release intensity of the functional groups reaches the maximum at 285 °C, with that for -C₆H₅ being 0.0049 a.u., -CH(CH₃)₂ being 0.0036 a.u., and -O- being 0.0029 a.u. For PL-WCCl, the release intensity of the functional groups also peaks at 285 °C, with that for -C₆H₅ being 0.0046 a.u., -CH(CH₃)₂ being 0.0043 a.u., and -O- being 0.0043 a.u. The release amounts of -CH(CH₃)₂ and -O- bond in PL-WCCl are more than those in PL-NMWCCl, which indicates that the Cu contained in 1 mm² of the blocky material can also accelerate the generation of lighter hydrocarbons.⁴¹

Fig. 6 presents the gaseous products at various pyrolysis temperatures. The range of 2327–2364 cm⁻¹ is the characteristic spectrum of the CO₂ gas;^{42,43} the 3015 cm⁻¹ band represents CH₄ gas, and the peak at 3742 cm⁻¹ is the stretching vibration of the -OH bond; thus, the range of 3855–3901 cm⁻¹ corresponds to H₂O.⁴⁴

Fig. 6 describes that when PL-NMWCCl and PL-WCCl undergo pyrolysis at different temperatures, the release of CO₂

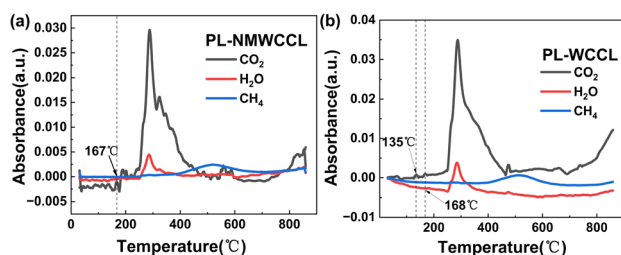


Fig. 6 FTIR of the gaseous products of pyrolysis at various temperatures: (a) PL-NMWCCl and (b) PL-WCCl.

and H₂O reaches the maximum at approximately 300 °C. After experiencing a period of decline, from 700 °C, the release of CO₂ continues to increase rapidly, and the release amount of PL-WCCl is slightly higher than that of PL-NMWCCl. The maximum absorbance of CO₂ for PL-NMWCCl is 0.0301 a.u., while for PL-WCCl, it is 0.0357 a.u. The release of CH₄ reaches the maximum at around 500 °C, but no peaks of HCl and HBr are present. The beginning pyrolysis temperatures of PL-WCCl and PL-NMWCCl are 135 °C and 167 °C, respectively, which means that the presence of Cu would decrease the beginning temperatures of pyrolysis and increase the amount of CO₂ released.^{42,43,45} This is also consistent with the conclusion drawn from the thermogravimetric curves.

3.2 The pyrolysis of PL-WCCl

3.2.1 Influence of pyrolysis conditions on metal-separation efficiency. Fig. 7 presents the metal separation rate of PL-WCCl after conducting pyrolysis at various temperatures and different retention times in a rotary furnace. As indicated in Fig. 7, when the pyrolysis temperature is 150 °C and the retention time is 60 min, the metal separation rate S_m is 100%, while at the same temperature, when the retention time is 30 min, the metal separation rate is merely 54.68%. As the pyrolysis temperature rises from 150 °C to 350 °C, the metal separation rate remains at 100% with a retention time of 60 min, while with a retention time of 30 min, the metal separation rate increases along with the pyrolysis temperature and reaches 100% at 350 °C.

Fig. 8 depicts the influence of different furnace types and raw material dosages on the metal separation rate of PL-WCCl at a pyrolysis temperature of 150 °C and a retention time of 60 minutes. As illustrated in Fig. 10b, the metal separation rate in the fixed furnace is merely 16.7%, while it is 100% in the rotary furnace, suggesting that the rotation of the rotary furnace is the primary factor for the separation of metals from non-metals. When the dosage of PL-WCCl is 30 g and 100 g, the metal separation rate is 100%, and the loading capacity of the rotary furnace at this time is 51.95 g L⁻¹. Conversely, when the dosage of PL-WCCl is increased to 150 g, the metal separation rate decreases to 74.57%.

Table S2 presents a summary of the published literature about the separation of the metal and non-metal components of

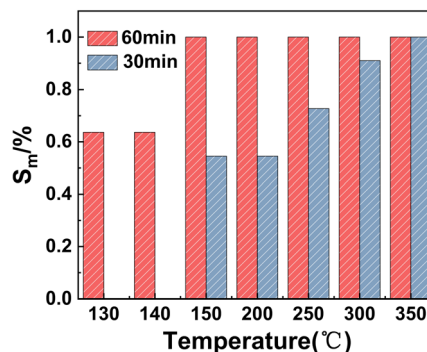


Fig. 7 Influence of the pyrolysis temperature and retention time on the metal separation rate of PL-WCCl.

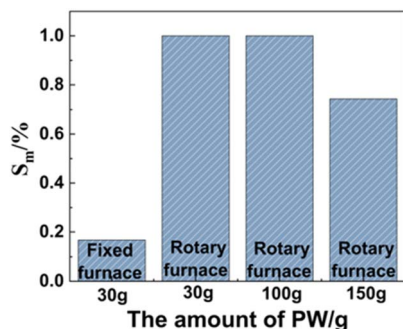


Fig. 8 Influence of the furnace type and dosages on the metal separation rate of PL-WCCL.

PL-WCCL through pyrolysis, encompassing the processing conditions, reactor types, subsequent steps needed and the metal separation rate achieved. Obviously, when the conditions of the stirring function for the reactor and a high processing temperature of 800 °C are available, the subsequent steps, including crushing or peeling off manually, are not necessary to complete the separation of the metal from the non-metal. Moreover, compared to other emerging low-temperature processes (such as organic solvent methods and combined processes), the proposed method requires less time, exhibits lower energy consumption, and generates minimal pollution. Compared with the physical method⁴⁶ in Fig. 9a, the pyrolysis in the rotary furnace is capable of not only automatically separating the metals and non-metals of PL-WCCL under 150 °C but also of reducing the number of processing steps from six to two (Fig. 9b). Furthermore, when compared to the physical method for separating metals and non-metals in WPCB, the low-temperature rotary process can reduce energy consumption by at least 70%.^{47,48}

3.2.2 Yield distribution of the gas–liquid–solid three-phase pyrolysis products of PL-WCCL. The yield distribution of the gas–liquid–solid three-phase pyrolysis products of PL-WCCL at various temperatures ranging from 150 °C to 350 °C and different retention times is shown in Fig. 10. By comparing the distribution of these three-phase products at different retention times in Fig. 10a and b, it can be observed that the yield of the

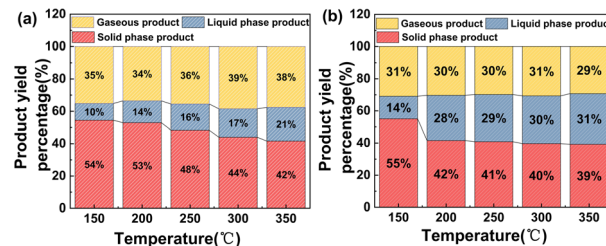


Fig. 10 Yield distribution of the gas–liquid–solid three-phase pyrolysis products of PL-WCCL: (a) retention time = 30 min and (b) retention time = 60 min.

gaseous products is 34–39% at a retention time of 30 min and 29–30% at 60 min. Thus, it can be concluded that the yield of the gaseous phase products is significantly influenced by the retention time, which is consistent with the literature conclusions of the research on the non-metallic powder of waste printed circuit boards alone.⁴⁹ The yield of the liquid phase products is 10–21% at a retention time of 30 min and 14–31% at a retention time of 60 min, which means a longer retention time results in an increase in the amount of liquid phase products.⁴ At a retention time of 60 min, the yield of the solid-phase products is 55% at a final temperature of 150 °C and drops to 39% if the final temperature increases to 350 °C, indicating that the heat decomposition of the insulating paper contained in the PL-WCCL leads to a lower solid-phase yield compared to that for PL-WCCL with glass fibres as its reinforcing material.⁵⁰

3.3 Product analysis of pyrolysis

3.3.1 GC-MS analysis of liquid-phase products. Fig. 11a shows the photographs of the liquid-phase products of PL-WCCL with a retention time of 60 minutes at different pyrolysis temperatures. Fig. 11b and Table S3 represent the analysis results of the GC-MS of the liquid-phase products. It can be observed from Fig. 11a that the liquid phases obtained at pyrolysis temperatures of 150 °C and 200 °C are clear and transparent, while as the pyrolysis temperature rises, the color of the liquid-phase products deepens. It is known from Table S3 that the main component of the liquid-phase products at different pyrolysis temperatures is phenol.^{45,51} It can be seen from the comparison of the relative content in Fig. 11b that the composition of the liquid-phase products becomes more and more complex when the pyrolysis temperature increases, and

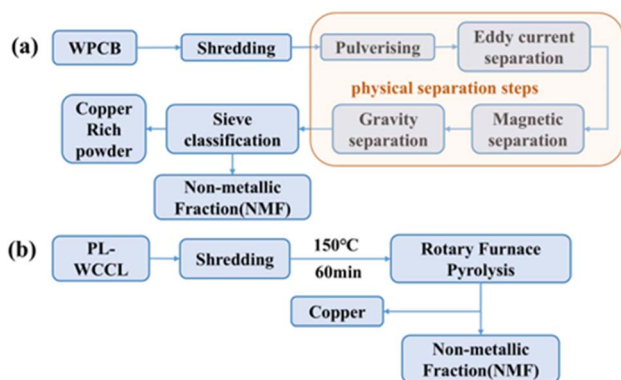


Fig. 9 Separation steps of metals from non-metals: (a) separation steps of the physical method for WPCB and (b) pyrolysis steps in a rotary furnace for PL-WCCL.

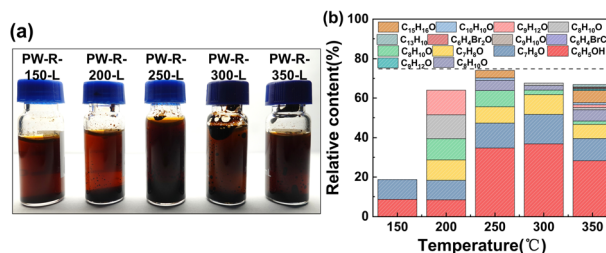


Fig. 11 Pyrolysis of PL-WCCL with a retention time of 60 min: (a) liquid products at various temperatures; (b) relative content (%) of the main component screened by GC-MS in liquid products.



halogen-containing organic compounds emerge at 350 °C. Since the screening of the main components is based on the criterion that the peak area is greater than 0.03,⁵² halogen-containing organic compounds were not observed at the final temperature of 300 °C. Fortunately, the liquid organic products obtained at the pyrolysis temperature of 150 °C are only phenol and *o*-cresol, which are of crucial importance for the subsequent clean utilization of the materials.⁵³

3.3.2 Morphological analysis of raw materials and solid pyrolysis products. Fig. 12 presents the photographs of the solid products of PL-WCCL, PL-NMWCCCL, and their solid pyrolysis products at different temperatures for 60 minutes. It can be observed from Fig. 12 that after the originally flat and dense PL-WCCL was heated in a rotary furnace, the shape of the non-metal bends, bubbles emerge on the unbonded metal surface, and the number of bubbles increases with the temperature. The delamination between layers becomes more obvious, and the contact surface with the metal shows a matte color and is prone to detachment. The metal surface becomes wrinkled and has a larger area than the non-metal part. The morphology of the solid pyrolysis product after the separation of the metal and the non-metal parts is completely different from that of the PL-WCCL subjected to thermal shock treatment.²¹

The morphology and the EDS spectrum analysis of the contact surfaces of both sides after manual delamination of the metal and non-metal in PL-WCCL are depicted in Fig. 13. As shown in Fig. 13a, the surface of the delaminated Cu foil consists of bright dots and lamellar structures. Through EDS analysis of the entire area, it can be observed that the granular bright dots in the figure are copper particles. The elements of bromine and chlorine are distributed densely and uniformly, with a bromine–chlorine ratio of 1 : 3, and 13.5% of the non-metal residue is present on the surface of the Cu foil in this area. It can be obtained from Fig. 13b that the non-metal is tightly bonded with a dense internal structure. The elements of bromine and chlorine are distributed evenly and densely. The bromine–chlorine ratio is consistent with that in the metal, and elements such as sodium, silicon, and iron are also detected.

Fig. 14 is the SEM images of the contact surfaces between the metal and non-metal parts of PL-WCCL after the pyrolysis for 60 min at various temperatures. Fig. 14a–e depict the SEM

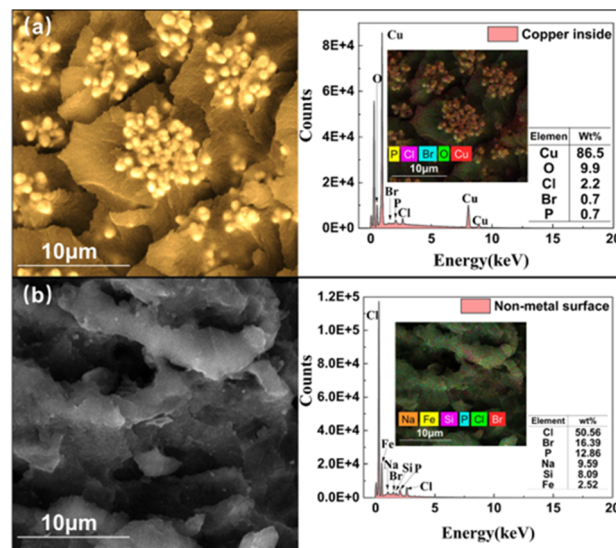


Fig. 13 SEM-EDS spectrum of PL-WCCL: (a) copper inside and (b) non-metal surface.

images of the contact surfaces of the metal part of PL-WCCL in the temperature range of 150 °C to 350 °C, and Fig. 14f–j represent the SEM images of the contact surfaces of the non-metal part at the same range of temperature. It can be observed from Fig. 14a–e that with the increase in the pyrolysis temperature, an increasing amount of the inner metal surface is exposed, and the adhesion of non-metal is gradually reduced, thereby weakening the bond between the metal and the non-metal in PL-WCCL.^{21,54} As shown in Fig. 14f and g, the surface of the non-metal is no longer densely adhered but assumes a honeycomb-like structure. The separation of the resin layer and the insulating paper layer is visible in Fig. 14h–14j. Further, even in the SEM images of the non-metal part at 250 °C and 300 °C, the fibrous structure within the insulating paper can be discerned after the epoxy resin layer has peeled off. This indicates that during the pyrolysis process, the non-metal undergoes decomposition and produces gas, which forms a number of bubbles at the contact surface of the metal and non-metal parts. Due to the malleability of the metal and the different properties of the metal and non-metal, the bubbles lead to a decline in the adhesive force at their contact surface. Further, under the influence of gravity and centrifugal force within the rotary furnace, separation can occur at a lower temperature during the pyrolysis process.

The SEM images of the cross-section of the non-metal part of PL-WCCL before and after pyrolysis at 150 °C in a rotary furnace are presented in Fig. 14k and l, respectively. The longitudinal section of the original non-metal part of PL-WCCL is compact and intact, while after being subjected to pyrolysis, its longitudinal section exhibits distinct stratification. This indicates that during the pyrolysis process, the cross-linking effect between the layers of epoxy resins is weakened due to the gas generated, resulting in the reduction of the adhesive force between the insulating paper layers and the macroscopic stratification phenomenon.

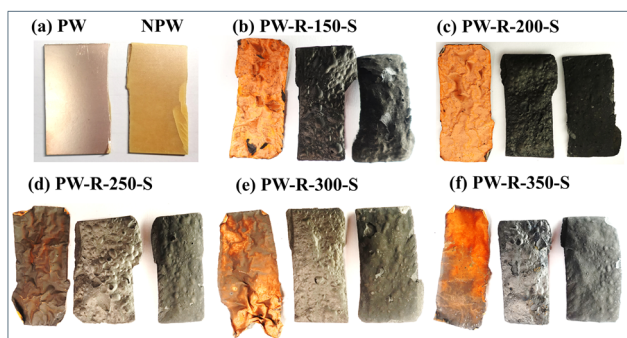


Fig. 12 (a) The metallic and non-metallic surfaces of PL-WCCL; the metallic and non-metallic parts of PL-WCCL obtained through rotary furnace heat treatment at different temperatures: (b) 150 °C, (c) 200 °C, (d) 250 °C, (e) 300 °C, (f) 350 °C.



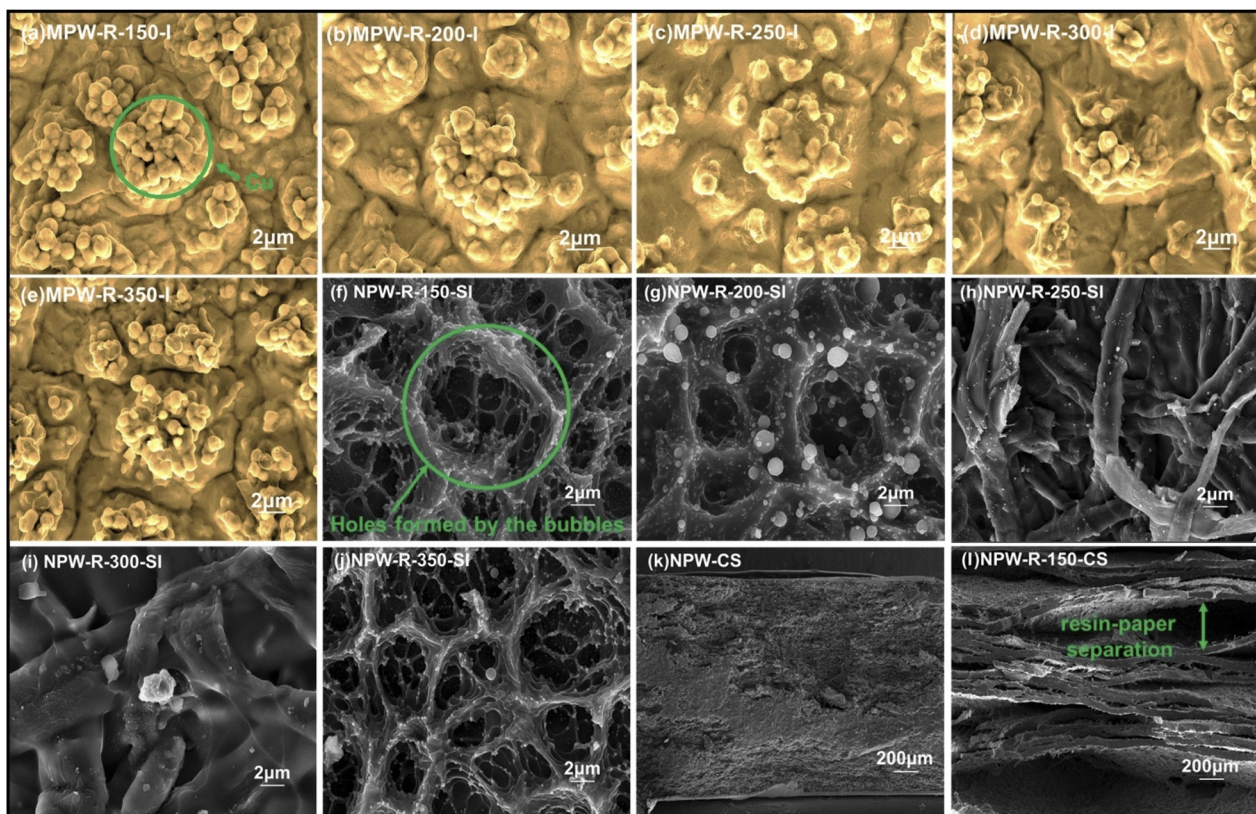


Fig. 14 SEM images of the contact surfaces of the metal part of the PL-WCCL at various temperatures (a–e); SEM images of the contact surfaces of the non-metal part of PL-NMWCCl at various temperatures (f–j); cross section of NPW (k); and cross section of NPW-R-150 (l).

4 Conclusions

In this study, the pyrolysis characteristics of PL-WCCL and PL-NMWCCl were analyzed using TG-FTIR analysis. It was discovered that the maximum weight loss rate of PL-WCCL was 62.48%, the activation energy E was 29.84 kJ mol^{−1}, and the pre-exponential factor A was $5.035 \times 102 \text{ min}^{-1}$; for PL-NMWCCl, the maximum weight loss rate was 66.51%, the activation energy E was 31.95 kJ mol^{−1}, and the pre-exponential factor A was $1.303 \times 103 \text{ min}^{-1}$. According to the 3D-FTIR spectra, the release patterns of the volatile products from PL-WCCL and PL-NMWCCl during pyrolysis are similar, both attaining the maximum release intensity around 288 °C. By comparing the release intensity of the characteristic functional groups of PL-WCCL and PL-NMWCCl at various temperatures, it is confirmed that the presence of Cu can lower the beginning reaction temperature, facilitate the release of bromine and chlorine, accelerate the synthesis of lighter hydrocarbons, and increase the release of CO₂. The rotary furnace is utilized to conduct the pyrolysis of PL-WCCL, and the separation rate of the metal can reach 100%, with a retention time of 60 min at 150 °C and a filling capacity of 51.95 g L^{−1}. In contrast, this percentage would decrease to 16.7% if the experimental device were switched to the fixed furnace and other experimental conditions remain unchanged. This outcome indicates that the influence of rotation is the main and crucial factor influencing the separation efficiency of metals and non-metals. Compared

with the physical method that is widely adopted in industry for the recovery of copper from WPCB, the creative process reduced the number of processing steps from six to two and simplified the procedures required. Comparing the gas–liquid–solid three-phase products with various retention times reveals that the yields of the gaseous and liquid-phase products increased when increasing the retention time from 60 min to 30 min, while the solid-phase product decreased. The liquid pyrolysis product of PL-WCCL at 150 °C was analyzed by GC-MS, and it was determined that there were only two organic compounds: phenol and *o*-cresol. Through photographing and SEM analysis of the morphology of the PL-WCCL solid-phase product, it was found that during the pyrolysis process in the rotary furnace, the gas generated by the decomposition of the non-metal formed a number of bubbles at the contact surface between the metal and non-metal. This resulted in a decrease in the bonding force between the metal and non-metal at the bonding point. Moreover, under the influence of gravity and centrifugal force, separation could occur at a relatively low temperature.

Author contributions

Meng Tian: conceptualization, methodology, investigation, visualization, writing – original draft, data curation. Xianglan Zhang: conceptualization, writing – review editing, project administration, funding acquisition, supervision.



Conflicts of interest

The authors declare that they have no known competing financial interests or personal relationships that could have appeared to influence the work reported in this paper.

Data availability

The data supporting this article have been included as part of the supplementary information (SI). Supplementary information is available. See DOI: <https://doi.org/10.1039/d5ra06865g>.

Acknowledgements

This work was supported by Guangdong Xingsheng Resource Recycling Co., Ltd (U0255).

References

- Q. Liu, J. Bai, R. Li, W. Gu, S. Peng, J. Wang, Z. Tang and C. Yu, *Bioelectrochemistry*, 2022, **144**, 108002.
- J. A. Conesa, N. Ortuño and A. Zielinska, *J. Anal. Appl. Pyrolysis*, 2017, **126**, 62–69.
- Financial Headline: Forecast and Analysis of China's Copper Clad Laminate (CCL) Production and Corporate Layout in 2025. <https://cj.sina.com.cn/articles/view/7962326780/1da9776fc0010168z0>, accessed June 2025.
- M. Haghi, F. Fotovat and S. Yaghmaei, *Waste Manag.*, 2023, **171**, 532–544.
- A. Kumar, M. Holuszko and D. C. R. Espinosa, *Resour. Conserv. Recycl.*, 2017, **122**, 32–42.
- J. Yang, H. Wang, G. Zhang, X. Bai, X. Zhao and Y. He, *Resour. Conserv. Recycl.*, 2019, **146**, 264–269.
- C. Guo, H. Wang, W. Liang, J. Fu and X. Yi, *Waste Manag.*, 2011, **31**, 2161–2166.
- S. B. Wath, M. N. Katariya, S. K. Singh, G. S. Kanade and A. N. Vaidya, *Chem. Eng. J.*, 2015, **280**, 391–398.
- S. Mir and N. Dhawan, *Resour. Conserv. Recycl.*, 2022, **178**, 106027.
- K. D. Kang, I. M. S. K. Ilankoon, N. Dushyantha and M. N. Chong, *Minerals*, 2021, **11**, 1134.
- H. Wang, G. Zhang, J. Hao, Y. He, T. Zhang and X. Yang, *J. Clean. Prod.*, 2018, **170**, 1501–1507.
- A. Otsuki, L. D. L. Mensbruge, A. King, S. Serranti, L. Fiore and G. Bonifazi, *Waste Manag.*, 2020, **102**, 510–519.
- Y. Chen, S. Liang, K. Xiao, J. Hu, H. Hou, B. Liu, H. Deng and J. Yang, *J. Clean. Prod.*, 2021, **280**, 124505.
- Q. Ma, *Preparation of activated carbon from non-metal waste circuit boards*, China University of Mining and Technology, Beijing, 2018.
- E. Ventura, A. Futuro, S. C. Pinho, M. F. Almeida and J. M. Dias, *J. Environ. Manage.*, 2018, **223**, 297–305.
- Z. Yao, M. Reinmüller, N. Ortuño, H. Zhou, M. Jin, J. Liu and R. Luque, *Prog. Energy Combust. Sci.*, 2023, **97**, 101086.
- M. Tian, Z. Liu, D. Ren, X. Zhang and C. Tie, *RSC Adv.*, 2025, **15**, 39417–39430.
- C. C. Wu, L. J. Bao, S. Tao and E. Y. Zeng, *Environ. Sci. Technol.*, 2016, **50**, 6599–6605.
- J. Guo, K. Lin, J. Deng, X. Fu and Z. Xu, *J. Hazard. Mater.*, 2015, **283**, 439–446.
- R. Qiu, M. Lin, B. Qin, Z. Xu and J. Ruan, *J. Clean. Prod.*, 2021, **279**, 123738.
- F. Liu, B. Wan, F. Wang and W. Chen, *J. Air Waste Manag. Assoc.*, 2019, **69**, 1490–1502.
- G. Yan, J. Guo, G. Zhu, Z. Zhang, P. Zhao, Z. X. Nan and B. Zhang, *Waste Manag.*, 2020, **106**, 145–154.
- B. Kim, S. Han, S. Park, S. Kim, M. Jung, C.-H. Park, H. S. Jeon, D. W. Kim and Y. Han, *Minerals*, 2021, **11**, 1213.
- X. Guo, F. G. F. Qin, X. Yang and R. Jiang, *J. Anal. Appl. Pyrolysis*, 2014, **105**, 151–156.
- L. Long, S. Sun, S. Zhong, W. Dai, J. Liu and W. Song, *J. Hazard. Mater.*, 2010, **177**, 626–632.
- H. Ma, N. Du, X. Lin, C. Li, J. Lai and Z. Li, *Sci. Total Environ.*, 2018, **633**, 264–270.
- M. Zhang, Y. Zhang, D. Ma, A. Li, W. Fu, G. Ji and J. Dong, *Chem. Eng. J.*, 2022, **445**, 136686.
- C. Ma, R. Zhu, Y. Ma, Y. Yu, C. Tan, S. Yang, H. Liu, J. Hu and H. Wang, *Biomass Bioenergy*, 2025, **193**, 107568.
- Y. Elkasabi, Y. Omolayo and S. Spatari, *ACS Sustain. Chem. Eng.*, 2021, **9**, 695–703.
- Y. Zhu, X. Wen, W. Zhang, F. Shen and Y. Cao, *Fuel*, 2025, **400**, 135717.
- L. Cao, P. Hu, X. Li, H. Su, J. Zhang and C. Zhang, *Carbon Neutrality*, 2023, **2**, 7.
- B. Li, B. Shen, R. Tao, C. Hu, Y. Wu, H. Yuan, J. Gu and Y. Chen, *Chin. J. Chem. Eng.*, 2024, **73**, 202–211.
- J. Liu, H. Zhang, Y. Xia, B. Hu, Z. Zhang, L. Zhao and Q. Lu, *Chem. Eng. J.*, 2025, **521**, 166695.
- H. H. Cebeci, K. Açikalin and A. K. Figen, *J. Mater. Cycles Waste Manag.*, 2023, **25**, 2205–2221.
- B. Boro and P. Tiwari, *Thermochim. Acta*, 2024, **736**, 179747.
- K. Açikalin, *Bioresour. Technol.*, 2021, **337**, 125438.
- Y. Wu, R. Tao, B. Li, C. Hu, W. Zhang, H. Yuan, J. Gu and Y. Chen, *Sci. Total Environ.*, 2024, **912**, 169610.
- T. Weidlich, *Catalysts*, 2021, **11**, 378.
- W. J. Liu, K. Tian, H. Jiang and H. Q. Yu, *J. Hazard. Mater.*, 2016, **310**, 217–225.
- C. Xu, *Organic Chemistry*, Higher Education Press, Beijing, 2nd edn, 2020.
- R. Gao, B. Liu, L. Zhan, J. Guo, J. Zhang and Z. Xu, *J. Hazard. Mater.*, 2021, **403**, 123465.
- Z. Zhan and K. Qiu, *J. Cent. South Univ.*, 2011, **18**, 331–336.
- J. Liu, Q. Jiang, H. Wang, J. Li and W. Zhang, *Chemosphere*, 2021, **280**, 130804.
- C. Zhou, Y. Zhang, X. Xing, T. Zhang, A. A. Siyal, Y. Liu, J. Dai, J. Qu, C. Liu, B. Yao, L. Chao, L. Chen, Y. Chen, J. Wang, J. Dong and L. Wang, *J. Clean. Prod.*, 2023, **421**, 138546.
- R. Gao, L. Zhan, J. Guo and Z. Xu, *J. Hazard. Mater.*, 2020, **383**, 121234.
- Y. Zheng, M. Ma and H. Shao, *Carbon Neutrality*, 2023, **2**, 23.
- Analysis of Energy Consumption in Waste Lithium Battery Crushing and Sorting Production Line: Cost Details and Process Impact for a 1 Ton/Hour Scale, <https://www.china->



- [tireshredder.com/a/news/xingyezshishi/2025/0909/373.html](https://www.tireshredder.com/a/news/xingyezshishi/2025/0909/373.html), accessed 9yue 2025.
- 48 Y. Chen, S. Liang, K. Xiao, J. Hu, H. Hou, B. Liu, H. Deng and J. Yang, *J. Clean. Prod.*, 2021, **280**, 124505.
 - 49 P. Ravi Raman, R. R. Shanmugam and S. Swaminathan, *Chem. Eng. J.*, 2024, **496**, 154339.
 - 50 Y. Zhang, C. Zhou, Y. Liu, J. Qu, A. Ali Siyal, B. Yao, J. Dai, C. Liu, L. Chao, L. Chen and L. Wang, *Waste Manag.*, 2024, **173**, 160–171.
 - 51 W. Chen, Y. Chen, Y. Shu, Y. He and J. Wei, *J. Clean. Prod.*, 2021, **313**, 127881.
 - 52 C. Quan, A. Li, N. Gao and Z. Dan, *J. Anal. Appl. Pyrolysis*, 2010, **89**, 102–106.
 - 53 Y. Liu, K. Liu, P. Wang, Z. Jin and P. Li, *Carbon Neutrality*, 2023, **2**, 14.
 - 54 T. Zhang, X. Mao, J. Qu, Y. Liu, A. A. Siyal, W. Ao, J. Fu, J. Dai, Z. Jiang, Z. Deng, Y. Song, D. Wang and C. Polina, *J. Hazard. Mater.*, 2021, **402**, 123749.

